Organic Electronics 13 (2012) 23–30

Contents lists available at SciVerse ScienceDirect

Organic Electronics

journal homepage: www.elsevier.com/locate/orgel

Efficient dye regeneration in solid-state dye-sensitized solar cells fabricated with melt processed hole conductors

Mindaugas Juozapavicius [a], Brian C. O'Regan [a,*], Assaf Y. Anderson [a], Juozas V. Grazulevicius [b], Viktorija Mimaite [b]

[a] Department of Chemistry, Imperial College London, Exhibition Road, London SW7 2AZ, United Kingdom
[b] Department of Organic Technology, Kaunas University of Technology, Radvilenu plentas 19, LT50254 Kaunas, Lithuania

ARTICLE INFO

Article history:
Received 28 June 2011
Received in revised form 27 September 2011
Accepted 29 September 2011
Available online 14 October 2011

Keywords:
Dye-sensitized solar cell
Melt-processable
Organic hole transporting material
Transient absorption spectroscopy

ABSTRACT

A new method for melting hole transporting materials (HTM) into mesoporous TiO_2 electrodes to obtain solid-state dye-sensitized solar cells (DSSC) is reported. Internal coverage is determined from the efficiency of hole conductor oxidation by photo-oxidized dyes (dye regeneration), measured using transient absorption spectroscopy. High efficiency regeneration indicates complete coverage of the electrode internal surface. A high work function hole conductor (>5.2 eV) was found to give shorter regeneration lifetimes (<1 μs) and better regeneration efficiencies (>90%) than expected. Cell photocurrents were low, but improved after iodine vapor doping of the hole conductor. Counter intuitively, doping also reduced the recombination rate constant 7-fold. A solid state solar cell with power conversion efficiency of 0.075% at 1 sun is reported.

1. Introduction

Dye-sensitized solar cells (DSSC) as a low-cost and efficient alternative to conventional inorganic photovoltaics have been under development since 1991 [1]. For hole transport, an iodine/iodide redox couple dissolved in a volatile organic electrolyte is utilized. Alternative approaches, such as non-volatile ionic liquids [2], polymer electrolytes [3], conjugated polymer conductors [4] and small molecule hole transporting materials [5] (HTM) have been demonstrated. Devices utilizing a triphenylamine based spiro-OMeTAD as the HTM layer are still unrivaled as solid-state DSSCs, yielding 5% power conversion efficiency [6]. Several other triphenylamine [7–10], hydrazone [11] and pentacene [12] based compounds have been reported as alternatives, with efficiencies of 2%, 0.07% and 0.8%, respectively. Inorganic hole conductors such as CuI and CuSCN have demonstrated efficiencies in the 2–3% range [13,14].

In previous reports, HTMs have been deposited by various means, including thermal evaporation and from solution. Poor titania pore filling has been reported as a major performance limiting factor in all cases. Various studies have indicated that for solution-deposited spiro-OMeTAD, or CuSCN the pore filling fraction is never more than 70% for oxide films $\leqslant 2$ μm, and drops off rapidly for thicker films [14,15]. This poor pore filling limits the photocurrent available from these cells. An alternative approach that could circumvent the pore filling problem would be the use of a solvent-free, melt-processable hole conductors to infiltrate the mesoporous titania. One previous study has pursued this approach [16]. Scanning electron microscopy was used to show that high pore-filling was obtained, however a low efficiency (0.04% at 0.1 sun) was reported. The authors did not attempt to include the standard additives used in high efficiency OMeTAD cells such as tert-butyl pyridine, lithium salts and chemical oxidants. Presence of these compounds in the HTM layer is vital in order to obtain efficient devices [17]. Solvent-free incorporation of ionic and chemical dopants into melt deposited HTM phase is a challenging task and in this paper we begin to address this issue. Using new melt-processable hole conductor we

* Corresponding author. Tel.: +44 (0) 207 594 5031; fax: +44 (0) 207 594 5801.
E-mail address: b.oregan@imperial.ac.uk (B.C. O'Regan).

1566-1199/$ - see front matter © 2011 Elsevier B.V. All rights reserved.
doi:10.1016/j.orgel.2011.09.024

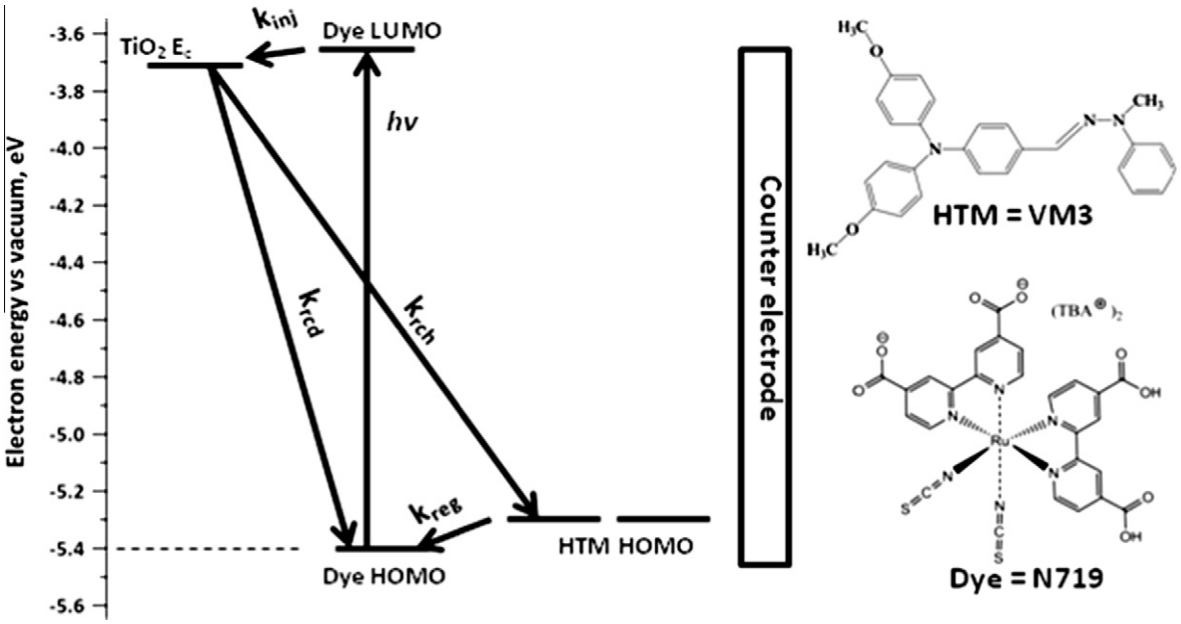

Fig. 1. Energy level diagram of a dye-sensitized solar cell. Arrows indicate the charge transfer processes. VM3 hole conductor and N719 dye structures are also indicated.

demonstrate high efficiency regeneration of the photo-oxidized dye molecules, indicated good pore filling or at least good surface coverage of all pores. Initial attempts to incorporate lithium salts and doping increase both the photocurrent and photovoltage of these cells, resulting in an increase of efficiency over the previous report.

Fig. 1 is an energy level diagram of the different dye-sensitized solar cell components and the fundamental charge transfer processess. Upon light absorption, an electron is excited from the HOMO to the LUMO of the dye molecule. The electron is then injected (k_{inj}) into the conduction band of TiO_2. The resulting photo-oxidized dye can then be regenerated (k_{reg}) by an HTM or it can recombine with the injected electron (k_{rcd}). After dye regeneration, charge transport is competing against electron recombination (k_{rch}) with a hole in the HTM layer. The energy values of TiO_2 conduction band edge and dye HOMO/LUMO levels were recently summarized elsewhere [18]. For comparison energy levels vs. NHE have been converted to vs. vacuum with NHE set at −4.4 eV relative to vacuum. In this report, transient absorption spectroscopy (TAS) is utilized to study regeneration yield and recombination kinetics.

2. Experimental

2.1. Device fabrication

Reagents $TiCl_4$·2THF, acetylacetone, titanium iso-propoxide, tris(4-bromophenyl)aminium hexachloroantimonate (TBPA), lithium bis(trifluoromethanesulfonimide) (LiTFSI), coumarin (1,2-benzopyrone) and solvents were purchased from Sigma–Aldrich and used without further purification. TiO_2 paste was prepared following published recipe [19,20]. N719 was kindly provided by Prof. M. Gratzel's group in EPFL, Switzerland. Synthesis and physical properties of the hole conductor VM3 (Fig. 1) will be reported separately [21]. The work function of VM3 was determined by ultraviolet photoelectron spectroscopy and was found to be 5.26 eV.

FTO/TiO_2/dye films were prepared as previously [22]. In brief, a glass plate covered with a thin film of SnO_2:F (TEC15, 15 Ω/□, Pilkington) was washed with a detergent, rinsed with deionized water and iso-propyl alcohol, dried and heated at 450 °C in air for 30 min. Thin film of TiO_2 blocking layer was deposited by spray pyrolysis of 0.4 M Ti(acetoacetonate) solution in ethanol at 450 °C with air flow [23]. After cooling down to room temperature, TiO_2 paste was applied by doctor blading using 50 μm scotch tape as a spacer. After drying in air for 30 min, the films were sintered at 450 °C for 30 min, giving 5 μm thick TiO_2 films as determined by profilometry. A $TiCl_4$ post-treatment was then carried out by immersing the films into a solution of 0.84 g $TiCl_4$·2THF in 80 mL of deionized water for 30 min at 70 °C. Substrates were then washed with deionized water and sintered for 30 min at 450 °C and cut into 1.5 × 2.5 cm pieces. Surrounding TiO_2 was scraped off to give 1 cm^2 active area, then heated again at 450 °C for 30 min and while still hot (∼100 °C) immersed into a 0.3 mM solution of cis–bis(isothiocyanato)bis(2,2′-bipyridyl-4,4′-dicarboxylato)ruthenium(II) (N719) dye in 1:1 mixture of acetonitrile:tert-butyl alcohol for 16 h.

2.2. Melting and doping

A dye-sensitized mesoporous titania electrode with TiO_2 area of 1 cm^2 was covered with a 1 mm thick glass plate which was just wide enough to cover the TiO_2 film.

Table 1
Summary of solar cell parameters.

Device	J_{sc} (μA cm^{-2})	V_{oc} (V)	FF	PCE (%)	LiTFSI pre-treatment	Iodine vapour exposure time (min)
A	24	353	0.26	0.002	No	2
B	130	560	0.34	0.025	Yes	5
C	332	521	0.43	0.075	Yes	15
D	473	270	0.33	0.042	No	80

This plate was held down lightly with a screw clamp. HTM powder was then added next to the glass strip/electrode junction and the device was transferred to a hot-plate in a nitrogen glovebox in order to avoid HTM oxidation. It should be noted, however, that it was not established if the nitrogen atmosphere is necessary. It was not checked if the HTM melt oxidizes in air. The substrate was heated at a temperature slightly higher than the HTM melting point, 134 °C for the VM3 used herein. As the HTM powder melted it was drawn into the space between the glass plate and the TiO_2 film. In approximately 2 min the whole TiO_2 active area was covered. The clamp was then tightened to force the glass plate closer to the TiO_2 film. This was done to minimize the HTM overlayer outside the TiO_2, which contributes to the series resistance of the cell. Without the tightening step, HTM overlayers of ~10 μm are obtained, whereas with tightening it is reduced to 0–2 μm. In some cases coumarin (CM) was used as an inert meltable material that would not regenerate the dye, but would provide a similar history and chemical environment in the pores to provide blank samples for transient absorption measurements.

The glass strip was removed after the electrode had cooled down. UV–Vis absorption was recorded before and after the melt infiltration to monitor any dye degradation. No changes in the dye absorption spectrum were observed after heating/melting, except for higher optical density due to presence of VM3. In order to p-dope the hole conductor, the electrode was transferred into a vial containing a few iodine crystals and the vial was sealed. The hole conductor was observed to darken immediately. Doping was carried out for fixed times as specified in Table 1. After doping a pressed graphite electrode was applied to the hole conductor overlayer to complete the solar cell. Schematic illustrating a finished device is shown in Fig. 2. In some cases 20 μL of 10 mM LiTFSI in acetonitrile was drop-cast on top of dye-sensitized TiO_2 prior to melting in the HTM.

2.3. Characterization

All the measurements were recorded in air at room temperature, unless indicated otherwise. Current–voltage curves were recorded using a Keithley 2400 Source Meter. A Xenon lamp fitted with an AM1.5 global filter was used for illumination. Silicon photodiode was used to calibrate the light source to give 1 sun light intensity. Voltage was cyclically sweeped from 0 to 1 V and to −1 V under illumination or in the dark.

Transient absorption spectroscopy was conducted using a pump–probe system similar to that reported previously [24]. Probe light was Bentham IL1 lamp output attenuated with neutral density filters to give roughly 1 sun light intensity (~100 mW cm^{-2}). Light was focused onto the sample and subsequently onto a monochromator. The photodetector had a rise time of 100 ns and was connected to a Costronics 2008 amplifier which was further connected to an oscilloscope with a time resolution of 4 ns. At least 20 laser pulse repeats per probe wavelength were used for averaging. The pump signal was supplied by an Nd:YAG 1064 nm light pumped OPO (Opotek Opolette 355) with 10 Hz repetition rate, 6 ns pulse duration. A waveguide was used to direct and decollimate the laser light. Excitation wavelengths were 460 nm for dye/coumarin and 510 nm for dye/VM3 samples. Pulse energy was roughly 0.026–0.04 mJ cm^{-2}. At early time scattered laser light was subtracted from the TA spectrum. During scattered light measurement the probe light was blocked and white background illumination was provided by 12 white LEDs (Luxeon LXHL-NWE8). Sample temperature was monitored to be at 27–30 °C. All samples used for TAS had very similar optical densities and film thicknesses in order to make the absolute absorptions comparable.

To obtain the optical absorption spectrum of VM3 cation a small amount of VM3 compound was dissolved in chlorobenzene and an equivalent amount of TBPA or iodine was added to obtain the oxidized form of VM3.

3. Results and discussion

3.1. Melting and solar cell performance

Filling the capillary space between the TiO_2 electrode and the covering glass sheet was observed to proceed easily and reproducibly using VM3, other hole conductors

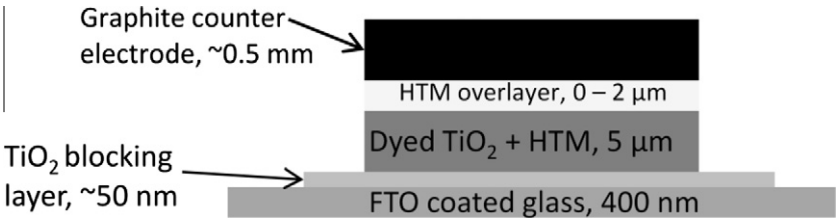

Fig. 2. Final device structure schematic indicating component thicknesses.

such as commercially available N,N′-Bis(3-methylphenyl) - N,N′-bis(phenyl)benzidine and 1, 3, 5-Tris[(3-methylphe nyl)phenylamino]benzene and other non-hole conducting substances such as Coumarin. However, of the three above mentioned HTMs only VM3 gave any photocurrent. Based on data presented in the next section, it seems that the hole conductors filled the pore space of the TiO_2, or at least coated the interior of most pores. Without iodine doping, the cells essentially showed no photocurrent. With iodine doping the conductivity of the hole conductor increased, as judged from the forward bias dark currents in Fig. 5. Iodine penetrated the HTM matrix and oxidized the hole conductor as confirmed by UV–Vis absorption spectroscopy, illustrated in Fig. 3. This implies that by oxidizing the hole conductor, free charges are introduced into the film which can carry the current. With the increased conductivity a photocurrent was observed.

Incident photon to current conversion efficiency (IPCE) was recorded of a cell with N719 dye and VM3 melted in, doped with iodine vapour for 15 min. The spectra is given in Fig. 4. Overlaid is absorbance spectrum of TiO_2 sensitized with N719, recorded in air. The two curves show significant overlap, indicating that the current does come from the absorption of the N719 dye. The IPCE spectrum is broader, indicating that more scattering occurred in the cell with VM3 and iodine doping.

Current–voltage curves at approximately 1 sun are given in Fig. 6. The IV parameters are collected in Table 1. We presume that the effect of iodine doping is in large part due to increasing conductivity of the hole conductor overlayer as under illumination the hole conductor in the pores should be photodoped. The addition of LiTFSI by itself increased both the photocurrent and photovoltage, although

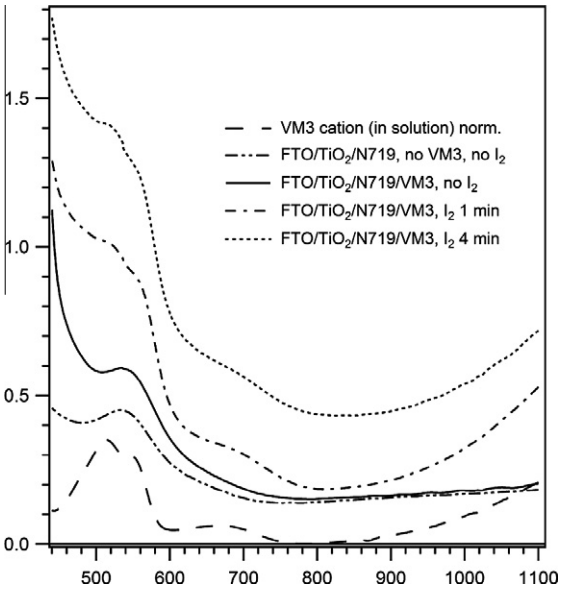

Fig. 3. UV–Vis absorption spectra of N719 sensitized TiO_2 samples filled with VM3 and at different iodine doping levels. Increasing the iodine doping time results in appearance of more VM3 cations. Iodine doping did not change the main spectral features.

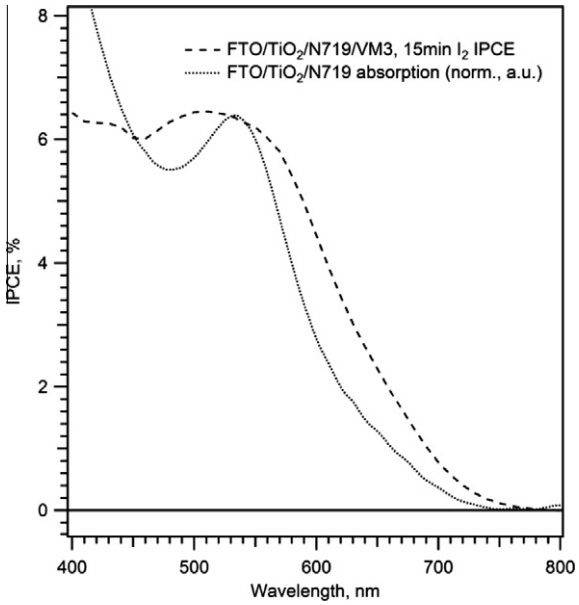

Fig. 4. Incident photon to current conversion efficiency of a FTO/TiO_2/N719/VM3/Graphite cell, doped for 15 min in iodine vapour. Overlaid is a normalized absorption spectrum of the same film before adding the HTM and iodine doping. It can be concluded that the photoaction is due to the dye absorption.

it must be noted that both Li and doping time were changed in the samples compared.

Solar cells doped with iodine for 15 min had the highest power conversion efficiency (0.075%). Devices which had 20 μL of 10 mM LiTFSI drop-cast prior to HTM deposition had ~250 mV higher photovoltage. The overall cell performances reported herein are still quite poor, and there may be several reasons for this. The most likely one is slow charge transport, as seen from the dark currents above. Another is fast charge recombination, as will be shown below. These two factors significantly retard the amount of charge which is able to reach the counter electrode and contribute to the photocurrent.

Addition of lithium salts is a widely employed performance enhancing method [25], but the mechanism for the improvement is inconclusive. However, it was found that lithium salts may significantly slow down the charge recombination [26]. They were also found to affect the interfacial energetics and influence the charge separation kinetics in solid-state DSSCs [7].

3.2. Transient absorption spectroscopy

Transient absorption spectroscopy (TAS) was employed to study photoinduced charge transfer kinetics in HTM melt-infiltrated TiO_2 films. During the TAS measurements samples were also illuminated with ~100 mW cm^{-2} white bias light to mimic operating conditions of a solar cell. In the absence of a counter electrode this is equivalent to the open-circuit condition of a full cell Fig. 7. shows difference spectra of three infiltrated TiO_2/N719 films recorded 3 μs after the laser pulse. The Figure also shows a control

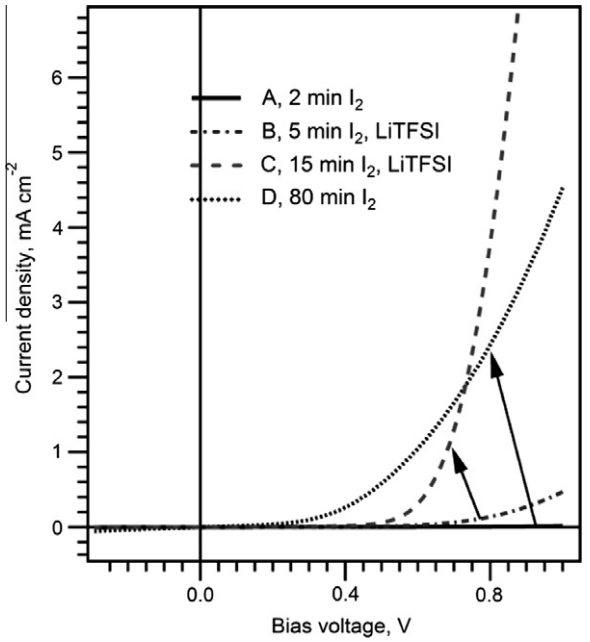

Fig. 5. Current–voltage curves of the four solar cells (FTO/TiO_2/N719/VM3/Graphite) in the dark. Increasing the iodine doping time improved the conductivity of the HTM layer, as seen from the increased forward bias current.

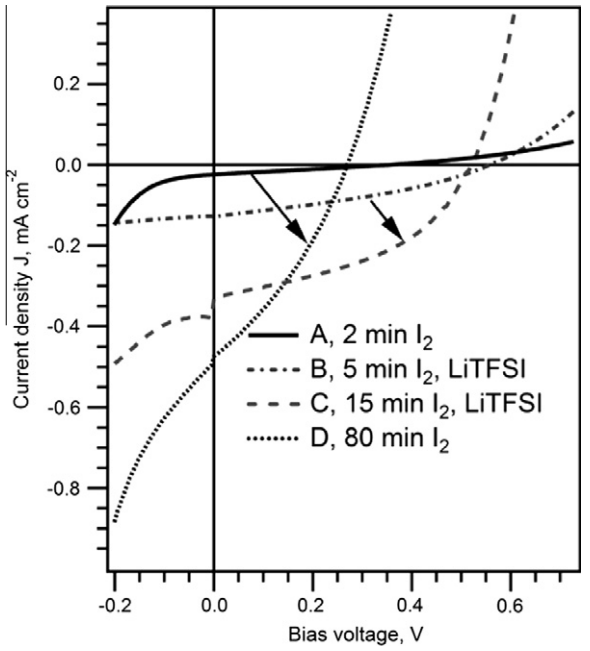

Fig. 6. Current–voltage characteristics of dye-sensitized solar cells (FTO/TiO_2/N719/VM3/Graphite) with melted in hole conductor and different iodine vapour exposure times. Illumination with AM1.5G simulated sunlight, intensity 100 mW cm^{-2} and device active area of 1 cm^{-2}. Details of solar cell parameters are given in Table 1. Arrows indicate the effect of iodine doping. Cells A and B had LiTFSI drop-cast prior to HTM deposition.

film (N719/CM) which was infiltrated with a high work function material which does not regenerate the

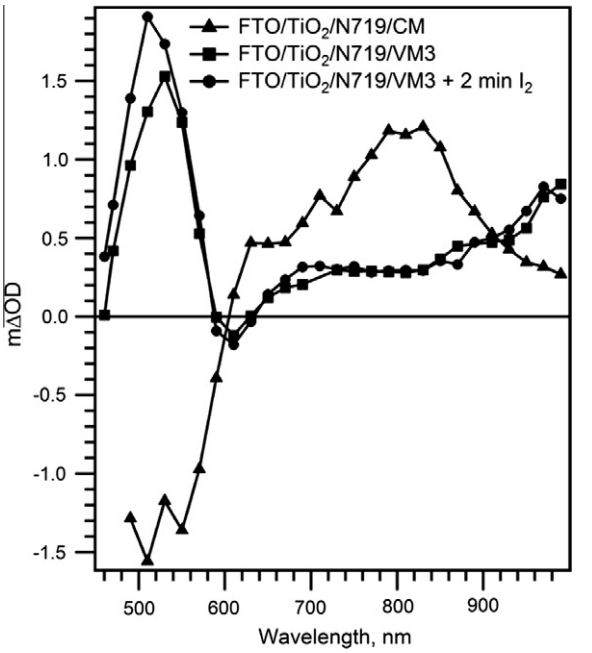

Fig. 7. Transient absorption spectra recorded 3 μs after laser pulse of 460 nm on FTO/TiO_2/N719/CM (triangles) and laser pulse of 510 nm on both FTO/TiO_2/N719/VM3 (squares) and FTO/TiO_2/N719/VM3 exposed to iodine vapour for 2 min (circles).

photo-oxidized dye, but does provide a chemical/physical environment similar to that when a hole conductor is present. Coumarin was chosen for this role due to its low-lying HOMO level, transparency at 400–1000 nm light and low melting point [27].

In the FTO/TiO_2/N719/CM spectrum in Fig. 7, the decrease of absorption at 490–600 nm corresponds to the bleach of the dye ground state. There is also likely a contribution from a Stark shift of the dye ground state absorption towards the blue [28,29]. The Stark shift would add to the apparent bleach on the red side of the ground state absorption. The strong absorption at 700–900 nm, centered at 810 nm is attributed to the oxidized dye [30,31]. Electrons in the TiO_2 contribute to absorption at 700–990 nm [32]. The presence of oxidized dye and TiO_2 electrons, and the magnitudes of the signals, indicate that excited state electron injection from the dye into TiO_2 is not strongly reduced by the melt infiltration procedure. Replacing the inert coumarin with VM3 produced two changes in the spectrum (Fig. 7). The absorption centered at 810 nm is strongly reduced compared to N719/CM case, indicating the oxidized dye concentration is much lower in this sample. In addition, a strong absorption at 460–590 nm appears which is assigned to the VM3 cation as demonstrated in Fig. 8.

Fig. 8 shows the optical absorption spectrum of VM3 cation in solution in comparison to the TiO_2/N719/VM3 difference spectrum, reproduced from Fig. 7. The two spectra share the 460–590 nm feature, and the rising absorption beyond 800 nm. In Fig. 8, the expected absorption at 600–700 nm region by the VM3 cation is mostly masked by the apparent dye bleach due to Stark shift, as mentioned

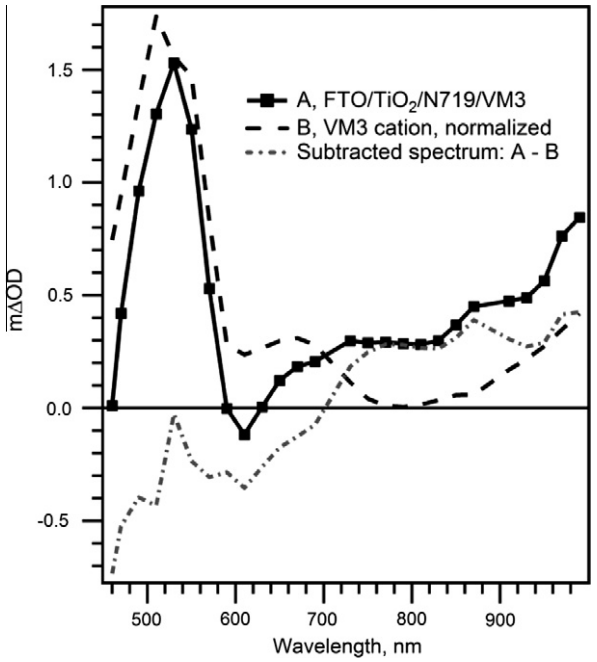

Fig. 8. Transient absorption spectra (3 μs after laser pulse) of FTO/TiO_2/N719/VM3 compared to the optical absorption of oxidized VM3 in solution. Solution spectra normalized to the transient at 520 nm. Also shown is subtraction of the normalized solution spectrum from the transient.

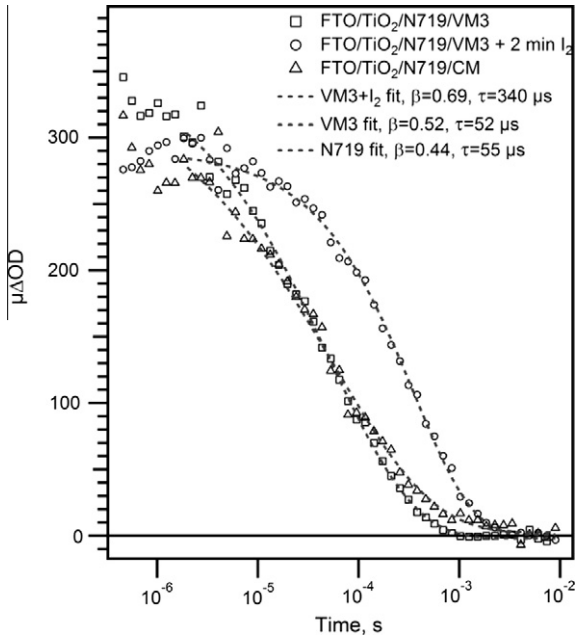

Fig. 9. Transient absorption decay of electrons in TiO_2 for three different devices. Decay of probe signal at 990 nm for FTO/TiO_2/N719/CM (triangles), at 810 nm for FTO/TiO_2/N719/VM3 (squares) and at 810 nm for FTO/TiO_2/N719/VM3 +2 min iodine vapour exposure (circles). Stretched exponential fitted electron lifetimes for the three devices were 55, 52 and 340 μs, respectively.

above. Subtracting the contribution of oxidized VM3 from the TiO_2/N719/VM3 spectrum (normalized at 520 nm) produces the dash-dot spectrum (A–B) in Fig. 8. On the red side, the remaining signal resembles the visible and NIR absorption of electrons in TiO_2. There appears to be virtually no contribution from oxidized dye molecules, implying that the regeneration of oxidized N719 by VM3 is complete by 3 μs. At 810 nm, the ratio of the oxidized dye signal in N719/CM to the electron signal in TiO_2/VM3 is four. This is essentially the same as that seen in N719/electrolyte cells where ~100% regeneration can be shown to occur by photocurrent efficiency [33]. Thus we can assume here that near 100% of the photo-oxidized dyes have been regenerated by VM3.

Fig. 7 also contains the TAS spectrum of a TiO_2/N719/VM3 electrode exposed to iodine vapour for 2 min. The spectrum is almost identical with the undoped sample spectrum. It appears iodine doping did not significantly alter injection and regeneration yields. If the iodine doping gives rise to free iodide in the hole conductor film, regeneration of the oxidized dye by iodide might occur, transiently re-creating iodine. The slightly larger absorption in the region of 500 nm might be an indication of iodine formation but much more data would be required to establish this.

Electron recombination to the oxidized dye in the N719/CM, and electron recombination to the hole conductor in N719/VM3 samples are examined in Fig. 9. The transient absorption wavelength for each sample was chosen to represent almost entirely the electrons in TiO_2. Thus we chose 980 nm for the TiO_2/CM sample, where there is no hole conductor contribution, but 810 nm for the TiO_2/VM3 samples where 980 nm appears to have a contribution from $VM3^+$ as well. The signal at 810 nm would also contain the oxidized dye if any, but as shown in Fig. 7, there is no remaining oxidized dye by 3 μs. The transient decays were fit with a stretched exponential function ($\Delta OD \approx A\exp[-(t/\tau)^{\beta}]$) and fitting parameters are indicated in Fig. 9. In TiO_2/N719/CM the recombination lifetime to the oxidized dye is about 50 μs, similar to that found for inert electrolyte cells (where no regeneration occurs) [33]. Interestingly, the electron/hole recombination in TiO_2/N719/VM3 is almost identical, implying the dye layer by itself does not block recombination, and perhaps that, after regeneration, the $VM3^+$ hole is trapped near the surface analogous to the situation in polymer/PCBM solar cells [34]. Contrary to expectation the iodine doped sample showed a 7-fold slower recombination. One might expect the increase in hole concentration in the VM3 to increase recombination, analogous to increasing the iodine in an electrolyte cell, however, the opposite happens. The effect is not fully understood.

The decays in Fig. 9 further indicate that the regeneration of the oxidized dye by VM3 is probably faster than 100 ns. If the regeneration was between 100 ns and 3 μs, one would expect a biphasic decay at 810 nm with the early decay reflecting regeneration. Although the data is noisy, there is no such decay seen. The initial amplitude of the oxidized dye signal would be on the order of 1.2 mOD as in Fig. 7, four times higher than that shown in Fig. 9. Thus we can conclude that regneration by VM3 is

substantially faster than 100 ns. That agrees well with similar studies where pico to nanosecond regeneration by an organic hole conductor was observed [35]. The kinetic data shown above imply a very high level of penetration of the pores by the melt infiltrated hole conductor, consistent with efficient dye regeneration.

The effect of iodine doping is twofold. It oxidizes the hole conductor and possibly introduces free charges into the HTM film, effectively improving conductivity of the organic layer. As discussed above, it also retards the recombination rate to oxidized species. The mechanism of the latter effect is unknown and is also counter-intuitive, as with a higher concentration of oxidized HTM molecules one would expect to obtain a faster charge recombination rate.

Solar cells without iodine doping had fast charge recombination rate and very low conductivity of the organic layer. Two minutes of iodine vapour exposure resulted in significant reduction of recombination rate, but only minor improvement in solar cell short-circuit current and overall performance. Further vapour exposure improved the HTM conductivity and photocurrent ten-fold up to almost 500 $\mu A\ cm^{-2}$, but these samples were unavailable for TAS studies as they became opaque. Further research to understand the limiting factors of these solar cells is in progress and new venues for improvement of melt-processed DSSCs are being explored.

4. Conclusions

A novel meltable hole transporting material and a reproducible melting method have been reported. Transient absorption spectroscopy experiments showed quantitative dye regeneration and implied complete wetting of the dye-sensitized TiO_2. Chemically doping the HTM layer increased its conductivity and was found to decrease charge recombination rate. Power conversion efficiency of 0.075% at simulated 1 sun illumination was obtained for the best device. It was demonstrated that melt-processing HTMs is an alternative option to infiltrate mesoporous nanocrystalline electrodes with compounds which otherwise might not be available for deposition from solution or thermal evaporation. Very low pure HTM conductivities and fast charge recombination rates were found to be the main performance limiting factors.

Acknowledgements

Xiaoe Li is greatly thanked for assistance. M.J. would like to acknowledge EPSRC for a Plastic Electronic Materials Doctoral Training Center studentship. Financial support by the Research Council of Lithuania (Project No. MIP-64/2010) is gratefully acknowledged.

References

[1] B. Oregan, M. Gratzel, A low-cost, high-efficiency solar-cell based on dye-sensitized colloidal TiO_2 films, Nature 353 (1991) 737–740.
[2] N. Papageorgiou, Y. Athanassov, M. Armand, P. Bonhote, H. Pettersson, A. Azam, M. Gratzel, The performance and stability of ambient temperature molten salts for solar cell applications, J. Electrochem. Soc. 143 (1996) 3099–3108.
[3] A.F. Nogueira, J.R. Durrant, M.A. De Paoli, Dye-sensitized nanocrystalline solar cells employing a polymer electrolyte, Adv. Mater. 13 (2001) 826–830.
[4] K. Murakoshi, R. Kogure, Y. Wada, S. Yanagida, Fabrication of solid-state dye-sensitized TiO_2 solar cells combined with polypyrrole, Sol. Energy Mater. Sol. Cells 55 (1998) 113–125.
[5] U. Bach, D. Lupo, P. Comte, J.E. Moser, F. Weissortel, J. Salbeck, H. Spreitzer, M. Gratzel, Solid-state dye-sensitized mesoporous TiO_2 solar cells with high photon-to-electron conversion efficiencies, Nature 395 (1998) 583–585.
[6] M. Wang, J. Liu, N.-L. Cevey-Ha, S.-J. Moon, P. Liska, R. Humphry-Baker, J.-E. Moser, C. Grätzel, P. Wang, S.M. Zakeeruddin, M. Grätzel, High efficiency solid-state sensitized heterojunction photovoltaic device, Nano Today 5 (2010) 169–174.
[7] J.E. Kroeze, N. Hirata, L. Schmidt-Mende, C. Orizu, S.D. Ogier, K. Carr, M. Grätzel, J.R. Durrant, Parameters influencing charge separation in solid-state dye-sensitized solar cells using novel hole conductors, Adv. Funct. Mater. 16 (2006) 1832–1838.
[8] Y. Zhao, W. Chen, J. Zhai, X. Sheng, Q. He, T. Wei, F. Bai, L. Jiang, D. Zhu, Solid-state dye-sensitized photovoltaic device with newly designed small organic molecule as hole-conductor, Chem. Phys. Lett. 445 (2007) 259–264.
[9] S.A. Haque, T. Park, A.B. Holmes, J.R. Durrant, Transient optical studies of interfacial energetic disorder at nanostructured dye-sensitised inorganic/organic semiconductor heterojunctions, Chem. Phys. Chem. 4 (2003) 89–93.
[10] K.R. Haridas, J. Ostrauskaite, M. Thelakkat, M. Heim, R. Bilke, D. Haarer, Synthesis of low melting hole conductor systems based on triarylamines and application in dye sensitized solar cells, Synth. Met. 121 (2001) 1573–1574.
[11] R. Aich, F. Tran-Van, F. Goubard, L. Beouch, A. Michaleviciute, J.V. Grazulevicius, B. Ratier, C. Chevrot, Hydrazone based molecular glasses for solid-state dye-sensitized solar cells, Thin Solid Films 516 (2008) 7260–7265.
[12] G.K.R. Senadeera, P.V.V. Jayaweera, V.P.S. Perera, K. Tennakone, Solid-state dye-sensitized photocell based on pentacene as a hole collector, Sol. Energy Mater. Sol. Cells 73 (2002) 103–108.
[13] G.R.A. Kumara, S. Kaneko, A. Konno, M. Okuya, K. Murakami, B. Onwona-agyeman, K. Tennakone, Large area dye-sensitized solar cells: material aspects of fabrication, Prog. Photovoltaics Res. Appl. 14 (2006) 643–651.
[14] B. O'Regan, F. Lenzmann, R. Muis, J. Wienke, A solid-state dye-sensitized solar cell fabricated with pressure-treated P25-TiO_2 and CuSCN: analysis of pore filling and IV characteristics, Chem. Mat. 14 (2002) 5023–5029.
[15] I.K. Ding, N. Tetreault, J. Brillet, B.E. Hardin, E.H. Smith, S.J. Rosenthal, F. Sauvage, M. Gratzel, M.D. McGehee, Pore-filling of spiro-ometad in solid-state dye sensitized solar cells: quantification, mechanism, and consequences for device performance, Adv. Funct. Mater. 19 (2009) 2431–2436.
[16] K. Fredin, E.M.J. Johansson, T. Blom, M. Hedlund, S. Plogmaker, H. Siegbahn, K. Leifer, H. Rensmo, Using a molten organic conducting material to infiltrate a nanoporous semiconductor film and its use in solid-state dye-sensitized solar cells, Synth. Met. 159 (2009) 166–170.
[17] H.J. Snaith, L. Schmidt-Mende, Advances in liquid-electrolyte and solid-state dye-sensitized solar cells, Adv. Mater. 19 (2007) 3187–3200.
[18] A. Listorti, C. Creager, P. Sommeling, J. Kroon, E. Palomares, A. Fornelli, B. Breen, P.R.F. Barnes, J.R. Durrant, C. Law, B. O'Regan, The mechanism behind the beneficial effect of light soaking on injection efficiency and photocurrent in dye sensitized solar cells, Energy Environ. Sci. 4 (2011) 3494–3501.
[19] C.J. Barbé, F. Arendse, P. Comte, M. Jirousek, F. Lenzmann, V. Shklover, M. Grätzel, Nanocrystalline titanium oxide electrodes for photovoltaic applications, J. Am. Ceram. Soc. 80 (1997) 3157–3171.
[20] M.A. Anderson, M.J. Gieselmann, Q. Xu, Titania and alumina ceramic membranes, J. Membr. Sci. 39 (1988) 243–258.
[21] V. Mimaite, J. Ostrauskaite, D. Gudeika, J.V. Grazulevicius, V. Jankauskas, Structure–properties relationship of hydrazones containing methoxy-substituted triphenylamino groups, Synth. Met. 161 (2011) 1575–1581.
[22] B.C. O'Regan, K. Walley, M. Juozapavicius, A. Anderson, F. Matar, T. Ghaddar, S.M. Zakeeruddin, C.d. Klein, J.R. Durrant, Structure/function relationships in dyes for solar energy conversion: a two-atom change in dye structure and the mechanism for its effect on cell voltage, J. Am. Chem. Soc. 131 (2009) 3541–3548.
[23] W.W. Xu, R. Kershaw, K. Dwight, A. Wold, Preparation and characterization of TiO_2 films by a novel spray pyrolysis method, Mater. Res. Bull. 25 (1990) 1385–1392.

[24] A.Y. Anderson, P.R.F. Barnes, J.R. Durrant, B.C. O'Regan, Simultaneous transient absorption and transient electrical measurements on operating dye-sensitized solar cells: elucidating the intermediates in iodide oxidation, J. Phys. Chem. C 114 (2010) 1953–1958.
[25] X. Liu, W. Zhang, S. Uchida, L. Cai, B. Liu, S. Ramakrishna, An efficient organic-dye-sensitized solar cell with in situ polymerized poly(3,4-ethylenedioxythiophene) as a hole-transporting material, Adv. Mater. 22 (2010) E150–E155.
[26] H.J. Snaith, A. Petrozza, S. Ito, H. Miura, M. Grätzel, Charge generation and photovoltaic operation of solid-state dye-sensitized solar cells incorporating a high extinction coefficient indolene-based sensitizer, Adv. Funct. Mater. 19 (2009) 1810–1818.
[27] P.D. Wood, L.J. Johnston, Photoionization and photosensitized electron-transfer reactions of psoralens and coumarins1, J. Phys. Chem. A 102 (1998) 5585–5591.
[28] S. Ardo, Y. Sun, A. Staniszewski, F.N. Castellano, G.J. Meyer, Stark effects after excited-state interfacial electron transfer at sensitized TiO_2 nanocrystallites, J. Am. Chem. Soc. (2010).
[29] S.A. Haque, Y. Tachibana, R.L. Willis, J.E. Moser, M. Gratzel, D.R. Klug, J.R. Durrant, Parameters influencing charge recombination kinetics in dye-sensitized nanocrystalline titanium dioxide films, J. Phys. Chem. B 104 (2000) 538–547.
[30] J.E. Moser, D. Noukakis, U. Bach, Y. Tachibana, D.R. Klug, J.R. Durrant, R. Humphry-Baker, M. Gratzel, Comment on ''measurement of ultrafast photoinduced electron transfer from chemically anchored Ru-dye molecules into empty electronic states in a colloidal anatase TiO_2 film'', J. Phys. Chem. B 102 (1998) 3649–3650.
[31] Y. Tachibana, J.E. Moser, M. Gratzel, D.R. Klug, J.R. Durrant, Subpicosecond interfacial charge separation in dye-sensitized nanocrystalline titanium dioxide films, J. Phys. Chem. 100 (1996) 20056–20062.
[32] G. Redmond, D. Fitzmaurice, Spectroscopic determination of flatband potentials for polycrystalline titania electrodes in nonaqueous solvents, J. Phys. Chem. 97 (1993) 1426–1430.
[33] A.Y. Anderson, P.R.F. Barnes, J.R. Durrant, B.C. O'Regan, Quantifying regeneration in dye-sensitized solar cells, J. Phys. Chem. C 115 (2011) 2439–2447.
[34] T.M. Clarke, J.R. Durrant, Charge photogeneration in organic solar cells, Chem. Rev. 110 (2010) 6736–6767.
[35] U. Bach, Y. Tachibana, J.E. Moser, S.A. Haque, J.R. Durrant, M. Gratzel, D.R. Klug, Charge separation in solid-state dye-sensitized heterojunction solar cells, J. Am. Chem. Soc. 121 (1999) 7445–7446.